



Design of AgNPs -Base Starch/PEG-Poly (Acrylic Acid) Hydrogel for Removal of Mercury (II)

Atefeh Saberi¹ · Mohammad Sadeghi^{1,2} · Eskandar Alipour¹

Published online: 10 January 2020

© Springer Science+Business Media, LLC, part of Springer Nature 2020

Abstract

In the present study, we introduce the formation of Starch/PEG-poly (acrylic acid) hydrogel (St-PEG-AcAH) and nano-composite of AgNPs-base St-PEG-AcAH (AgNPs-St-PEG-AcANCH) free radical method, and their characterization using analytical techniques of FT-IR, TEM, SEM, EDX, AFM, XRD, TGA/DTG. The thermodynamic parameters and application of prepared hydrogels was investigated for the removal of Hg²⁺ ions in water and the various solvents such as ethanol-water (30:70), ethanol-water (50:50), 2-propanol–water (40:60), respectively. The maximum adsorption capacity of Hg²⁺ ions for St-PEG-AcAH and AgNPs-St-PEG-AcANCH was achieved 158.21 mg/g and 182.53 mg/g in pH 7 and 6 in aqueous solutions, respectively. On the other hand, the results of adsorption isotherms revealed that adsorption process for both adsorbents occurred as a homogenous and monolayer process with L-shape isotherm. Furthermore, investigating the bioactivity of bioadsorbents, the good antimicrobial efficiency of the prepared samples was confirmed on *E. coli* bacteria.

Keywords Nano composites · Hydrogels · Starch · Ag nanoparticles

Introduction

Even at trace levels, heavy metal ions are considered as a serious threat for both human beings and aquatic lives [1]. The rapid development of industrial wastewater containing heavy metal ions is known as a biohazard for human health and ecological systems [2] due to the dangerous impacts on living organisms, health, biodegradability, and accumulation. Among the heavy metals, Hg has unusual chemical and physical properties, which can act as a neurological and renal poison and easily pass the blood–brain barrier and affect the fetal brain [3]. Even at low percentages, Hg can cause severe hazards due to its strong diffusion into biological tissues. Numerous cases of mercury poisoning or Minamata disease are reported in different countries around the world for consumption of fish and shellfish living in polluted waters [4]. Therefore, it necessities the removal of these heavy metal ions from the waste waters before drainage. In the last few years, heavy metals have been

removed from aqueous media using many methods such as chemical precipitation, reverse osmosis, solvent extraction, ultrafiltration, ion exchange, electrochemical treatment, nanofiltration, coagulation and adsorption [5]. These techniques have a certain effect on the treatment of heavy metal ions. However, there is less report on the pollution treatment technology with the complete removal of heavy metals, low-energy requirements, availability of non-toxic sludge, high efficiency, normal operating conditions, and simple and economical disposal [6]. The majority of these advantages may have been reached using the adsorptive processes because of the simple and stable handling, high efficient treatment, the absence of secondary pollution and low operating cost [1]. Adsorption approach has been universally accepted as one of the most commonly applied technique for the removal of heavy metal ions and seems to pose a great impact on transport, toxicity and biological availability of trace amounts of heavy metals in aqueous media. Besides, it is easy to operate and cost effective [7]. From a practical point of view, however, many limitations have remained in the field of wastewater treatment. For example, the difficulty of separation and the issue of recyclability of bioadsorbents which make their industrial applications expensive [8]. In this respect, several efficient bioadsorbents have been used for wastewater treatment with high quality of adsorptive interactions and effective removal of target

✉ Mohammad Sadeghi
msadeghi_77@yahoo.com; m-sadeghi@iau-arak.ac.ir

¹ Department of Chemistry, Islamic Azad University, Tehran-North Branch, Tehran, Iran

² Department of Chemistry, Islamic Azad University, Arak branch, P.O. Box 38135-567, Arak, Iran

contaminants from wastewater effluents [9]. Mineral, organic or biological origins are more prospects for these bioadsorbents- e.g., activated carbons, zeolites, clay minerals, industrial by-products, agricultural waste, biomass, and polymeric materials [10]. One of the typical fascinating and versatile soft material with wide potential applications in the adsorption of heavy metals is a polymeric material, such as hydrogels. The network structure of hydrogels has attracted considerable attention due to their high water retention, tunable mechanical properties, self-degradation, and environmental applications [11], which has large application potential in the environment. Many researchers have been tried to prepare hydrogels with superior adsorption properties such as magnetic responsive composite based on AMPS for the removal of metal ions with high level of toxicities (Fe(II), Pb(II), Cu(II), Cd(II), Co(II), Ni(II), and Cr(III)) in aqueous environments [12] and selective removal of Hg^{2+} ions using a chitosan–poly (vinyl alcohol) hydrogel (CTS–PVA) [13]. Nanocomposite (NC) gels are considered due to their improved properties, for instance, the extraordinary mechanical property of organic–inorganic hybrid networks of nanocomposite gels [14]. Nano dispersions of metal nanoparticles are used to prepare nanocomposites due to their special properties such as the large surface area to volume ratio and multiple applications. In fact, incorporation of silver nanoparticles (AgNPs) into the hydrogels has developed both mechanical properties and chemical stability of hydrogels, as well as increasing the adsorption capacity. In addition, due to the antimicrobial properties of AgNPs, biocompatible polymers containing AgNPs have proven to be promising candidates for the biomedical area due to their superior antibacterial properties [15] beside their great ability in metal ions adsorption [16]. On the basis of these premises, we aimed to formulate a biocompatible nanocomposite hydrogel as bioadsorbent for metal ion removal in water and the various solvents such as ethanol–water (30:70), ethanol–water (50:50), methanol–water (40:60), respectively. In this work, we proposed a method to synthesize the novel starch-based/PEG–AcA hydrogel (St-PEG–AcAH) and novel AgNPs–starch/PEG–AcA nanocomposite hydrogel (AgNPs–St-PEG–AcANCH). To the best of our knowledge, there has no such reported on the synthesis of a novel nanocomposite hydrogel based on starch, poly ethylene glycol, acrylic acid and AgNPs for simultaneous investigation of antimicrobial activities and removal of metal ions from contaminated water solutions.

Materials and Methods

Materials

Soluble starch ($M = 342.30$) and poly ethylene glycol (PEG 4000, average molwt 1450 and $d = 1.0919 \text{ g/mL}$ at $60 \text{ }^\circ\text{C}$) were purchased from Sigma-Aldrich. Acrylic acid (AcA;

$M = 72.06 \text{ g/mol}$, $d = 1.06 \text{ g/cm}^3$) and ammonium persulfate (APS) were purchased from Fluka and used after vacuum distillation. N, N-methylene bis acrylamide (MBA) and mercury (II) nitrate were purchased from Merck and used as received. Nano silver liquid (20 nm, 99%) was purchased from Mehregan Chemistry company. Escherichia coli (ATCC-25922) strain was kindly donated by microbiology laboratory of Islamic Azad University, Tehran, Iran. All other chemicals used were of analytical grade and were used as received without further purification.

Synthesis of Starch-Based/PEG–AcA Hydrogel and AgNPs–Starch/PEG–AcA Nanocomposite Hydrogel

Briefly, starch (0.5 g) was solved in warm water at $80 \text{ }^\circ\text{C}$. After 15 min, MBA (0.05 g) was dissolved in water (5 mL) and added to the aqueous solution with continuous mechanical stirring (300 rpm) until a homogeneous viscous mixture was obtained. The reaction temperature was controlled at $65 \text{ }^\circ\text{C}$ under an argon atmosphere, then a certain amount of 70% neutralized AcA (6 mL), and PEG (0.24 g) was added to the reaction mixture. At the next step, a definite amount of APS solution (0.08 g) was added into the mixture and was stirred for 10 min until the hydrogel was produced. For the synthesis of AgNPs–St-PEG–AcANCH, the as-prepared AgNPs colloidal solutions (100–400 ppm) were mixed with the above homogeneous solution and allowed until the reaction was completed within 10 min. Then, after cooling to room temperature, the reaction was neutralized with a certain amount of alkaline solution. Afterward, the reaction mixture was left over night in ethanol (200 mL). In the last step, the samples were filtered and dried at $50 \text{ }^\circ\text{C}$. Also, the viscosity of synthesized AgNPs–St-PEG–AcANCH was determined using HVU 481 viscometer (Herzog Contracting Corp–Germany Model) about 2.45 cP at $20 \text{ }^\circ\text{C}$ in order to investigate the size distribution of AgNPs.

Characterizations

The morphology characteristics of synthesized samples were evaluated using field emission scanning electron microscopy (SEM, Hitachi S-4800). The thermo gravimetric analysis (TGA) was measured under a nitrogen atmosphere with a TG/DTA7300 from room temperature to $700 \text{ }^\circ\text{C}$ with the heating rate of $10 \text{ }^\circ\text{C/min}$. The functional groups of samples were detected using FT-IR American Nicolet 5700 spectrophotometer. The crystal phases of the samples were analyzed using X-ray diffractometer (XRD, M21X, MAC Science Ltd., Japan) with Cu-K α radiation. UV–Vis diffuse reflectance spectra (DRS) were recorded on a UV–Vis spectrophotometer (Cary 300, USA) with an integrating sphere. The chemistry of the surface of bioadsorbents was also determined using X-ray

photoelectron spectroscopy (XPS, K-Alpha 1063, Thermo Fisher Scientific, and England).

Adsorption Measurements

The Hg^{2+} removal capacity of St-PEG-AcAH and AgNPs-St-PEG-AcANCH from aqueous solutions was determined using a batch process with nitrate salts of Hg^{2+} . The batch experiments were applied for determining the adsorption of Hg^{2+} metal ions using shaking the flasks at 300 rpm for a constant period of time with a beaker shaker. St-PEG-AcAH (0.15 g) and AgNPs-St-PEG-AcANC (0.1 g) were thoroughly mixed with the analytical grade $\text{Hg}(\text{NO}_3)_2$ (200 ppm). After 60 min, the precipitates were removed by centrifuging. The centrifuge tubes were placed in an incubator shaker (QYC2112, Fuma, Shanghai, China) at the desired temperature and fixed rotating speed of 600 rpm for 1 h. Then, the initial and final concentrations of Hg^{2+} solution were monitored on an atomic absorption spectrophotometer (Z-2000, Hitachi, Japan). This procedure was repeated three times, and the average percentage values of extracted Hg^{2+} metal ions were calculated using Eqs. 1 and 2 [17]:

$$q_e = \frac{(C_0 - C_e)}{m} \times V \quad (1)$$

$$\%R = \frac{(C_0 - C_e)}{C_0} \times 100 \quad (2)$$

where the amount of Hg^{2+} (mg/g) adsorbed at equilibrium is defined by q_e . C_0 and C_e are the initial and equilibrium concentrations of Hg^{2+} (ppm), respectively. The mass of bioadsorbents (g) and the volume of the metal ion solution (L) are specified respectively by m and V .

Antibacterial Measurements

The potential of prepared hydrogel samples in the field of antibacterial properties was examined using agar diffusion method against a gram-negative *E. coli* as a model bacterium. In this method, the bacteria cultures were grown onto nutrient agar plates after sterilized by autoclaving for 1.5 h at 100 °C. Then, both hydrogel and nanocomposite hydrogel (0.1 g) was suspended in distilled water after sonication and loaded onto above nutrient agar plates. Incubation of the inoculated plates was done at 38 °C for 38 h, then, the diameters (mm) of the inhibition zones were determined in three directions, and the average was calculated.

Results and Discussion

Polymerization Procedure of St-PEG-AcAH and AgNPs-St-PEG-AcANCH

Free radical polymerization involved for stabilization of nanoparticles [18] has been used for the preparation of both bioadsorbents. The copolymerization started at 65 °C in a constant-temperature bath when APS was decomposed to make radical initiator by abstracting hydrogen from functional groups such as COOH, OH in a side chain of polymer. Random free radical polymerization of AcA and PEG monomers onto starch by sequential crosslinking method accomplished according to Table 1.

In fact, heating leads to the decomposition of APS as the thermal initiator and preparation of sulfate anion radical. Abstraction of hydrogen from one of the existing hydroxyl groups in starch and PEG backbone is occurred to form the corresponding macro-initiator on the substrate. The redox pairs systems, i.e. (starch- or PEG-APS) lead to copolymers initiated by radically active centers capable of initiated polymerization of AcA monomers. Subsequently, the presence of crosslinker (MBA) in the reaction mixture prepared a crosslinked structure as shown in Scheme 1.

Characterization of St-PEG-AcAH and AgNPs-St-PEG-AcANCH

FTIR Analysis

FTIR spectroscopy was employed to confirm the chemical structure of pure starch and the prepared bioadsorbents. Figure 1 showed the FTIR spectra of the prepared St-PEG-AcAH and AgNPs-St-PEG-AcANCH samples, respectively. As can be seen, the broad band at 3000–3600 cm^{-1} was related to the stretching vibration of OH groups on both starch and PEG polymers. The skeletal mode vibration of the glycoside linkage is illustrated at 900–950 cm^{-1} . In the spectrum of St-PEG-AcAH bioadsorbent, the new characteristic absorption peaks at 1621 and 1766 cm^{-1} were assigned to stretching of carboxamide and carbonyl groups in crosslinker and acrylic acid monomers, respectively. Meanwhile, in this graph, two other characteristics peaks of carboxylate ion were clearly visible for St-PEG-AcAH [19]. The first peak is at about 1403 cm^{-1} , assigned to the symmetric stretching mode of the carboxylate ion, while the second peak is at 1580 cm^{-1} due to the asymmetric stretching mode of COO^- groups. These results suggested that the grafted acrylic acid monomers were a presence in two forms of non-ionized (COOH) and ionized (COO^-) onto the polymer backbone [20]. The

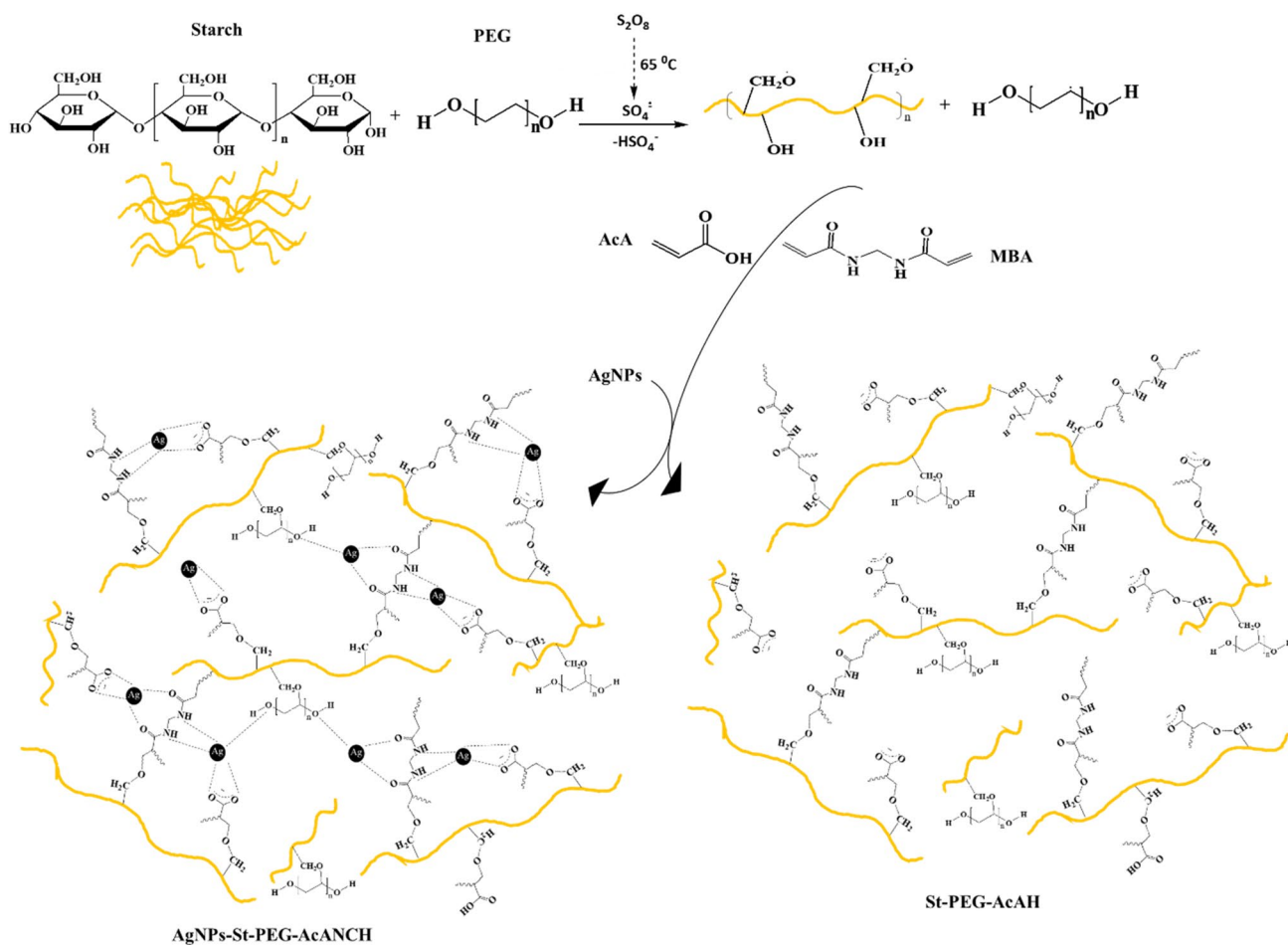
Table 1 Optimum contents and conditions in the synthesis of St-PEG-AcAH and AgNPs-St-PEG-AcANCH

	Starch (w/w)	PEG (w/w)	APS (mol L ⁻¹)	AcA (mol L ⁻¹)	AgNPs (ppm)	MBA (mol L ⁻¹)	Neutralization
St-PEG-AcAH	4	1.5	0.030	1.2	0	0.006	70%
AgNPs-St-PEG-AcANCH	4	1.5	0.030	1.2	400	0.006	70%

peak around 2962 cm⁻¹ and 1472 cm⁻¹ are also related to the CH stretching and bending mode. On the other hand, the FTIR spectrum of the nanocomposite hydrogel showed the same peaks but with a little shifting (Fig. 1). In other words, the characteristic features of the spectrum of the prepared nanocomposite were almost similar to those of the spectrum of the hydrogel but with this different that the several changing was happened. These changing contain the shifts in basic peaks position from 3465 cm⁻¹ to 3455 cm⁻¹ related to NH or OH groups, and 1766 cm⁻¹ to 1746 cm⁻¹ related to carboxylate groups where indicating the chelating O and N atoms of carboxylate and -NH₂ groups of AgNPs-St-PEG-AcANCH with Ag to form an interpenetrating network. However, the IR results indicated that no additional peak was formed in the FI-IR spectrum of the prepared nanocomposite, and this suggesting the interaction of AgNPs with hydrogel networks without any chemical bonding formation [21]. Therefore, we suggest that AgNPs are included in free-network spaces of hydrogels or anchored on the surface of hydrogels. However, from these finding preliminarily can be induced that the AgNPs-St-PEG-AcANCH nanocomposite had been synthesized.

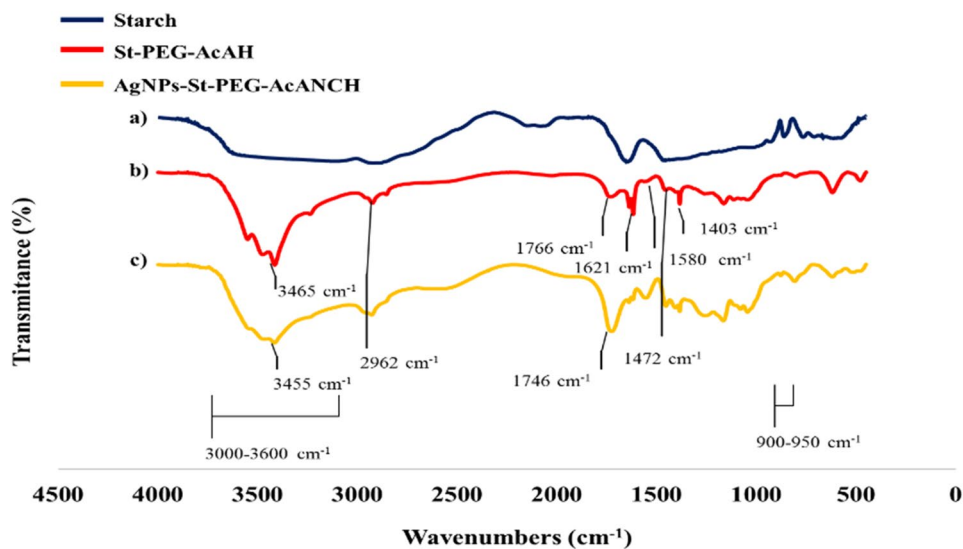
SEM, EDX, TEM and AFM Techniques

SEM, EDX, AFM and TEM techniques have been used to evaluate the incorporation of AgNPs into the St-PEG-AcAH matrix; the morphology and topography both of bioadsorbents and the results are showed in Fig. 2a–c. In Fig. 2a, it was clearly indicated that both of bioadsorbents had porosity structures, while the surface morphology of AgNPs-St-PEG-AcANCH was rougher than St-PEG-AcAH. In Fig. 2a, the presences of elements were illustrated in both bioadsorbents. The figure showed the elemental composition of bioadsorbents; it was calculated that AgNPs-St-PEG-AcANCH contained about 58.69% of carbon, 18.19% of oxygen, 17.68% of nitrogen, 5.02% of sodium, and 0.42% of silver. The results confirmed the deposition of Ag nanoparticles in the nanocomposite hydrogel matrix. In Fig. 2b, AFM images were depicted the surface morphology of the bioadsorbents. Comparing the 2D and 3D images in Fig. 2b, the surface morphology for St-PEG-AcAH was shown to be a smooth while for AgNPs-St-PEG-AcANCH nanocomposite was a rough surface with clustered features. The morphology, shape, and distribution of AgNPs size were determined by analyzing the TEM images of the nanocomposite hydrogel. The images of TEM was shown in Fig. 2c and confirmed a highly uniform distribution of the spherical AgNPs with the average of size particles ranges between 40–50 nm inside the nanocomposite hydrogel.



Scheme 1 Free radical polymerization, the plausible mechanism for the formation of AgNPs-St-PEG-AcANCH

Fig. 1 FTIR spectra of Starch (a); St-PEG-AcAH (b) and AgNPs-St-PEG-AcANCH (c)



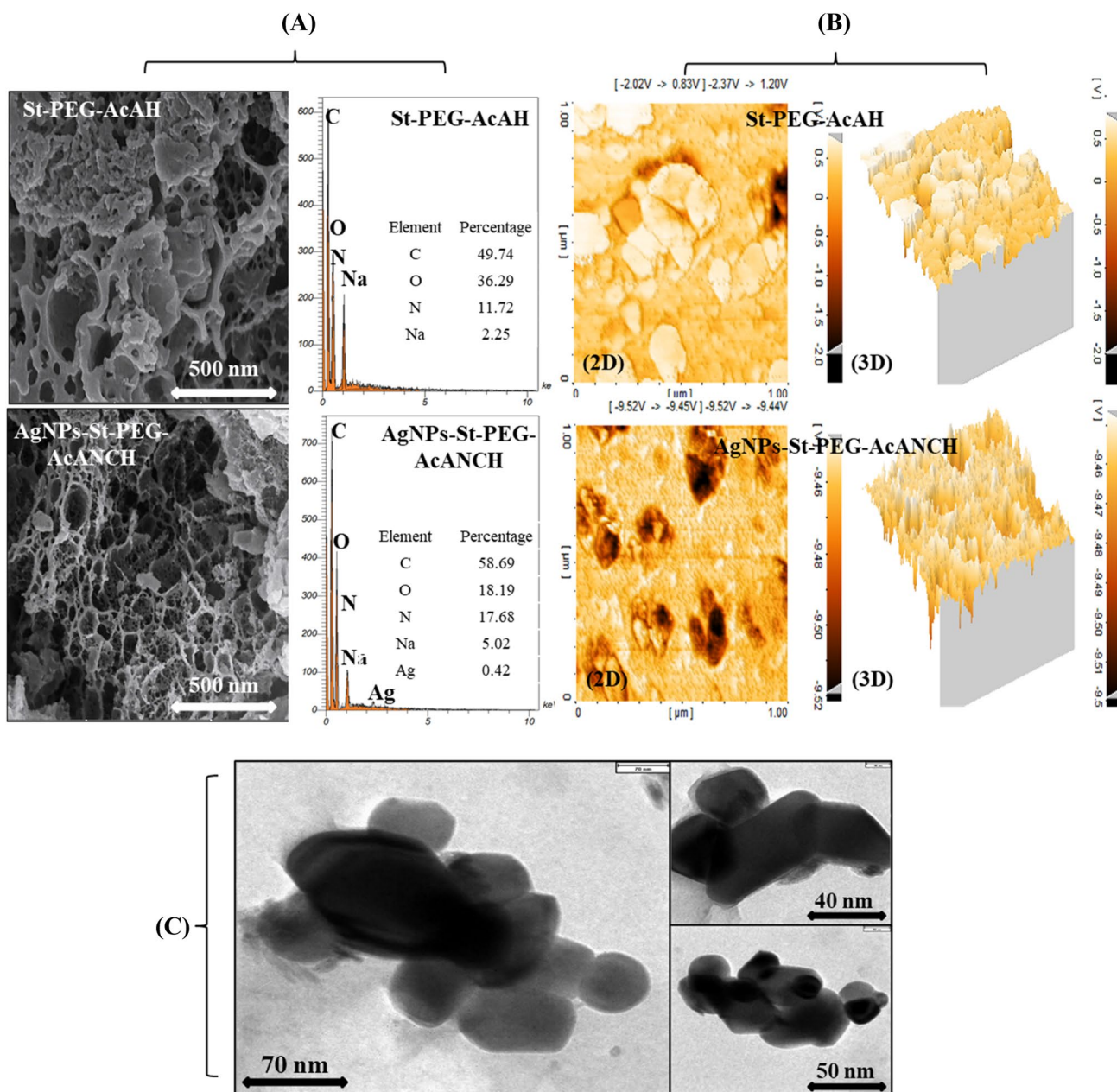


Fig. 2 The SEM images, EDX spectra of both prepared samples (a), The 2D and 3D AFM images of St-PEG-AcAH and AgNPs-St-PEG-AcANCH (b) and TEM images of the nanocomposite (c)

XRD Analysis

Analyzing the structure of both bioadsorbents using X-ray diffraction was illustrated in Fig. 3a. As shown in the XRD patterns, St-PEG-AcAH had no characteristics peaks, which confirmed its amorphous nature. In contrast, AgNPs-St-PEG-AcANCH exhibited relative sharp peaks at $2\theta = 57.1^\circ, 67.2^\circ$ and 102.34° which were assigned to planes of the silver structure. In addition, the slight

difference between XRD patterns of the nanocomposite and AgNPs can be concluded that the AgNPs into nanocomposite matrix were well crystallized. Furthermore, no peaks related to the impurities were observed in XRD patterns. The average particle size of the trapped AgNPs into the AgNPs-St-PEG-AcANCH Based on Debye-Scherrer equation was found about 45 nm with the good agreement with the results of AFM and TEM analysis [22].

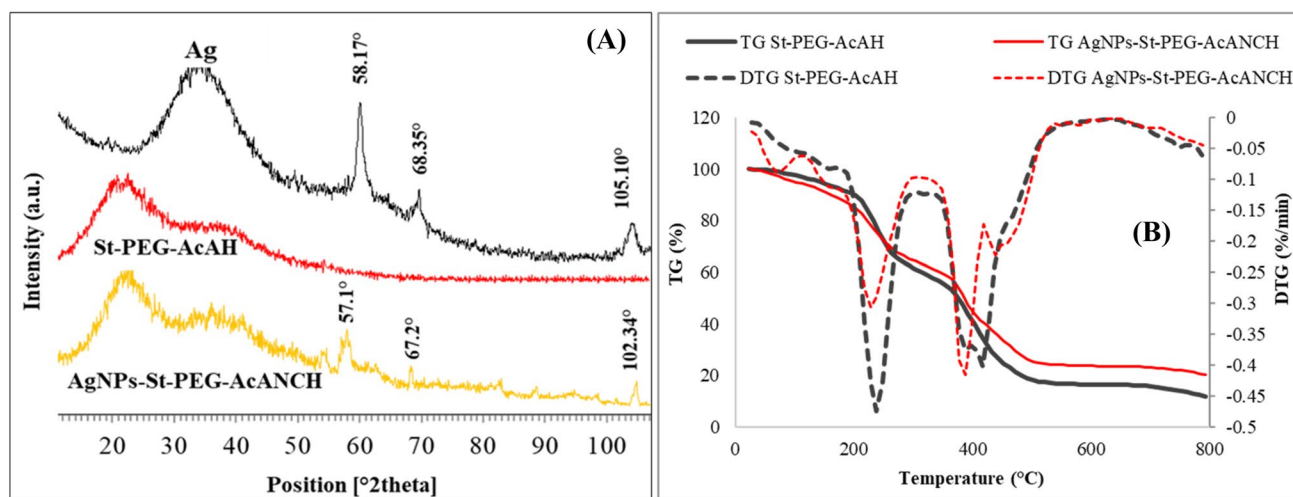


Fig. 3 The XRD patterns of Ag nanoparticles compared with St-PEG-AcAH and AgNPs-St-PEG-AcANCH (a), TGA and DTG profiles of St-PEG-AcAH and AgNPs-St-PEG-AcANCH (b)

TGA/DTG Analysis

Figure 3b represented the TGA/DTG analysis of both prepared bioadsorbents. Two steps of decomposition were seen for St-PEG-AcAH. The first weight loss at 150–250 °C was due to evaporation of adsorbed water and the second rapid weight loss was due to the thermal degradation of the organic content of St-PEG-AcAH structure in the range 400–500 °C. Similar decomposition steps were also seen for AgNPs-St-PEG-AcANCH. In addition, the total weight loss of AgNPs-St-PEG-AcANCH and St-PEG-AcAH was about 66% and 81% at 800 °C, respectively. According to these results and values of nanocomposite compared to St-PEG-AcAH such as 195.91 °C which was higher compared to that of the hydrogel, the higher thermal stability of AgNPs-St-PEG-AcANCH was concluded. The presence of silver nanoparticles might be the reason for this high thermal stability in the nanocomposite matrix [23].

Investigation of Effective Parameters onto Removal of Hg²⁺ Ions

Effect of Bioadsorbent Mass

Reaching the maximum Hg²⁺ removals, determining the optimal bioadsorbent mass loaded would be one of the important steps. Therefore, the range of 0.01–0.4 g was examined at 298 K and Hg²⁺ concentration of 200 ppm at equilibrium time 1 h to find the effects of amount bioadsorbents for removal of Hg²⁺ ions (Fig. 4a). It is observed that the increasing of the number of bioadsorbents resulted in an increase of Hg²⁺ percentage removals, with a maximum of 96.32% and 90.43% for AgNPs-St-PEG-AcANCH and

St-PEG-AcAH, respectively; however, the adsorption capacity of both bioadsorbents was decreased. It could be concluded that at the lower level of bioadsorbent content in the reaction mixture, there were more available active sites for trapping the metal ions, so the adsorption capacity for Hg²⁺ ions removal increased. At higher levels, the system reached equilibrium at lower concentrations of adsorbed metal ions indicating that the number of unsaturated active sites onto both bioadsorbents decreased [24, 25].

Effect of pH Solution

The effect of pH on the adsorption of Hg²⁺ ions at equilibrium time 1 h was investigated for both bioadsorbents, St-PEG-AcAH and AgNPs-St-PEG-AcANCH and the results are shown in Fig. 4b. To confirm the effectiveness of pH, adsorption of Hg²⁺ ions was performed in a 60-minute experiment while changing the initial pH of Hg solution from pH 2 to 9. It was considered that the good uptake of Hg²⁺ in the pH range of 5–7 was determined as a function of hydrogen ion concentration. At lower pH values, hydrogen ions are likely to compete with Hg²⁺ ions, and at higher pH values, Hg²⁺ ions were precipitated. The adsorption was maximized at pH 6. In general, the dependence of the adsorption to pH was indicated [26].

Effect of Hg²⁺ Concentration

The effect of the initial concentration of Hg²⁺ ions was evaluated in the range of 50–300 ppm at 298 K and at equilibrium time 1 h for St-PEG-AcAH and AgNPs-St-PEG-AcANCH. As illustrated in Fig. 4c, increasing the initial Hg²⁺ ions concentration from 50 to 300 ppm decreased

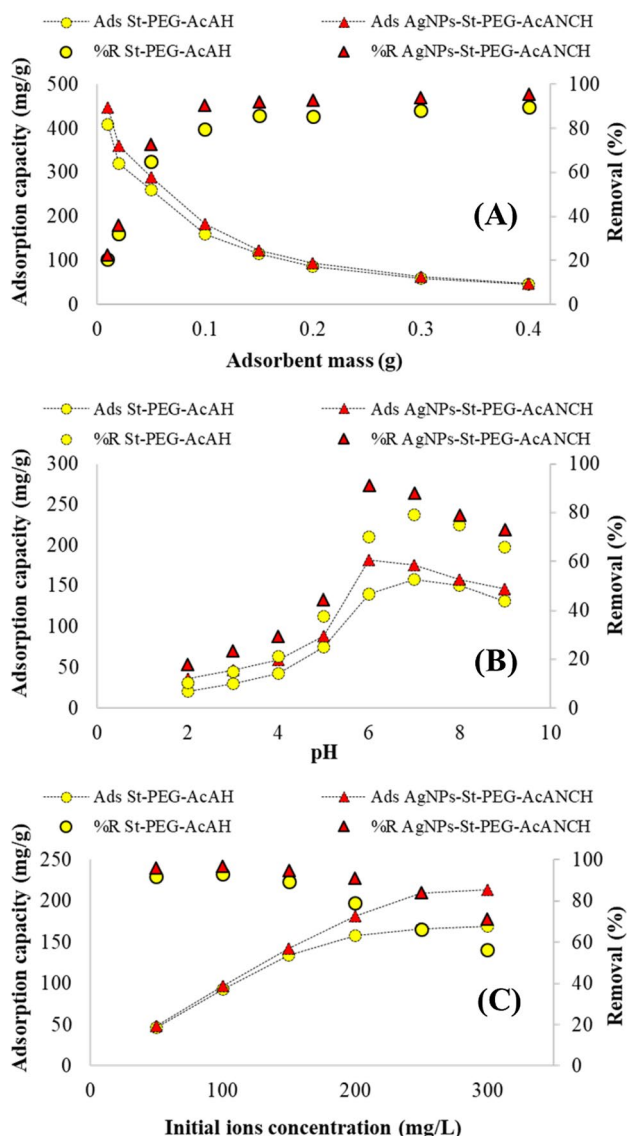


Fig. 4 Effect of the bioadsorbents mass (a), solution pH (b) and initial ion concentration (c) on Hg²⁺ ions adsorption capacity and % removal on both bioadsorbents

Table 2 The solvent–water concentrations and swelling-loss percentage of St-PEG-AcAH and AgNPs-St-PEG-AcANCH

Adsorbents	Solvent	δ_{mix}	Swelling-loss (%)	Adsorption capacity (mg g ⁻¹)
St-PEG-AcAH	H ₂ O/EtOH (70/30)	20.19	35	136.34
	H ₂ O/EtOH (50/50)	18.05	43	110.20
	H ₂ O/MeOH (60/40)	19.84	41	123.79
AgNPs-St-PEG-AcANCH	H ₂ O/EtOH (70/30)	20.19	32	170.84
	H ₂ O/EtOH (50/50)	18.05	46	119.12
	H ₂ O/MeOH (60/40)	19.84	39	137.53

Symbols δ [(cal/cm³)^{1/2}] for ethanol and methanol solvents is 12.7 and 14.5, respectively

the percentage removal ability of both bioadsorbent while increased the adsorption capacity. Further increasing Hg²⁺ ions concentration leads to the constant adsorption of Hg²⁺, which means more occupation or saturation in the active surface sites of bioadsorbents.

Effect of Solvents

In this section of our experiment, the swelling changes and thereafter adsorption capacity of the optimized hydrogel and nanocomposite for trapping Hg²⁺ ions were examined in mixtures of water and hydrophilic solvents such as ethanol–water (30:70), ethanol–water (50:50), methanol–water (40:60). As shown in Table 2, with adding organic solvents to water, the swollen hydrogels shrink and ultimately adsorption capacity decreased gradually so that, swelling-loss for ethanol-H₂O (30:70), and ethanol-H₂O (50:50), and methanol-H₂O (40:60), were 35, 43 and 41% for hydrogel, and 32, 46 and 39% for nanocomposite hydrogel, respectively, whereas the shrinkage of adsorption capacity in aforementioned solvents were 14, 30 and 21% for hydrogel, and 6, 35 and 24% for nanocomposite hydrogel, respectively. The reason of this shrinkage can be attributed to widely restriction of anionic groups onto polymer matrix in organic solvent–water systems because the organic solvent molecules cannot solvate the anionic groups. As a consequence, the swelling capacities and adsorption capacity of samples are considerably decreased. However, this swelling loss can be proportionate with $\delta_{water} - \delta_{mix}$ where this phrase is definite as the solubility parameter variations of the solvent–water mixtures [27]. In above equation, the solubility parameter for solvent–water mixtures (δ_{mix}) can be calculated using the Eq. 3.

$$\delta_{mix} = \delta_1\Phi_1 + \delta_2\Phi_2 \tag{3}$$

where Φ_1 and Φ_2 are the volume fraction, and δ_1 and δ_2 are the solubility parameters of the two solvents. According to the obtained results in Table 2, it can be seen that the maximum swelling capacity of the hydrogel and nanocomposite was obtained in water with the solubility parameter

of $23.4 \text{ (cal/cm}^3\text{)}^{1/2}$. On the other hand, with increasing of δ_{mix} values toward 23.4, the hydrogel can be highly swollen as in pure water. In other words, the swelling capacity of the hydrogel in the solvent water mixture will be close to that in pure water if $\delta_{\text{water}} - \delta_{\text{mix}} = 0$ [28].

The similar results have been observed in the hydrogel/water–solvent systems based on poly (acrylic acid)-attapulgit superabsorbent composites [29].

Investigation Of Thermodynamic Parameters

The effect of temperature on Hg^{2+} ions removal was carried out in the various solvents such as water, ethanol-water (30:70), ethanol–water (50:50), 2-propanol–water (40:60) and at three different temperatures 288 K, 298 K, and 308 K. The results are shown in Table 3. The thermodynamic parameters such as Gibb's free energy change (ΔG° , kJ/mol), enthalpy change (ΔH° , kJ/mol), and entropy changes (ΔS° , J/K mol) were estimated according to Eqs. 4 and 5:

$$\Delta G^* = -RT \ln K_c \quad (4)$$

$$\ln K_c = \frac{-\Delta H^*}{RT} + \frac{\Delta S^*}{R} \quad (5)$$

where R is the gas constant (8.314 J/mol K), $K_c = C_{Re}/C_{Se}$ is adsorption affinity, C_{Re} is the equilibrium concentration of the sorbed Hg^{2+} ions (ppm) and C_{Se} is the equilibrium concentration of the metal ions in the solution (ppm) and T is the temperature (K). The enthalpy change (ΔH°) and entropy change (ΔS°) were also calculated from the slope and intercepted of $\ln K_c$ versus $1/T$, respectively.

The more negative amounts of ΔG° for both bioadsorbents were seen at all investigated temperatures when water was selected as a solvent (Table 3). In addition, increasing the temperature from 288 to 308 K showed more effective sorption of Hg^{2+} ions on both of bioadsorbents at the highest temperature. On the other hand, by comparing ΔG° of St-PEG-AcAH ($-2.568 \text{ kJ mol}^{-1}$) and AgNPs-St-PEG-AcANCH ($-4.554 \text{ kJ mol}^{-1}$) can be found that kinetic of adsorption process for AgNPs-St-PEG-AcANCH was quicker than that of St-PEG-AcAH.

Table 3 Thermodynamic parameters of Hg^{2+} ions removal using St-PEG-AcAH and AgNPs-St-PEG-AcANCH

Adsorbents	Solvents	Temperature (K)	Thermodynamic parameters				
			K_c	$\Delta G \text{ (kJ mol}^{-1}\text{)}$	$\Delta H \text{ (kJ mol}^{-1}\text{)}$	$\Delta S \text{ (J mol}^{-1} \text{K}^{-1}\text{)}$	
St-PEG-AcAH	H_2O						
AgNPs-St-PEG-AcAH - AcA	H_2O	288	2.922	-2.568	18.944	74.623	
		299	3.763	-3.284			
		308	4.882	-4.062			
		$\text{H}_2\text{O}/\text{EtOH} \text{ (70/30)}$	288	1.778	-1.378	18.271	69.634
			299	2.125	-1.868		
			308	2.921	-2.746		
		$\text{H}_2\text{O}/\text{EtOH} \text{ (50/50)}$	288	1.020	-0.047	6.714	24.153
			299	1.083	-0.198		
			308	1.197	-0.462		
	$\text{H}_2\text{O}/\text{MeOH} \text{ (60/40)}$	288	1.223	-0.480	14.124	51.445	
		299	1.597	-1.160			
		308	1.857	-1.586			
	H_2O	288	6.692	-4.554	42.447	162.621	
		299	10.112	-5.735			
		308	21.223	-7.826			
	$\text{H}_2\text{O}/\text{EtOH} \text{ (70/30)}$	288	2.846	-2.894	38.621	144.148	
		299	4.003	-4.398			
		308	5.557	-5.774			
	$\text{H}_2\text{O}/\text{EtOH} \text{ (50/50)}$	288	1.083	-0.191	21.531	75.396	
		299	1.469	-0.953			
		308	1.941	-1.699			
	$\text{H}_2\text{O}/\text{MeOH} \text{ (60/40)}$	288	1.500	-0.971	33.852	120.577	
		299	2.174	-1.925			
		308	3.761	-3.394			

Adsorption Isotherm

Adsorption isotherms were utilized to explain the adsorption data by linear Langmuir and Freundlich isotherms. In these isotherms, the metal uptake per unit weight of the bioadsorbent q_e was related to the equilibrium concentration of adsorbate in the bulk fluid phase C_e . Purposing the design of sorption mechanism of Hg^{2+} ions onto both of bioadsorbents, the adsorption isotherms were used. Two classical adsorption models, i.e., Langmuir and Freundlich isotherms were studied to find the best isotherm model that would well fit with the experimental results obtained from the considered system. The Langmuir model describes saturated monolayer adsorption of solute molecules on a homogeneous site without any interaction between adsorbed ions. Unlike the Langmuir model, the Freundlich model describes the adsorption on heterogeneous surfaces with the interaction between adsorbed molecules [25]. The linear form of Langmuir and Freundlich isotherms are shown in Eqs. 6 and 7, respectively.

$$C_e/q_e = 1/(q_m b) + C_e/q_m \tag{6}$$

$$\log q_e = \log K + \left(1/n\right) \log C_e \tag{7}$$

C_e is the equilibrium concentration of Hg^{2+} metal ions in aqueous solution (ppm), q_e and q_m are the equilibrium

adsorption capacity and maximum adsorption capacity of the bioadsorbent ($mg\ g^{-1}$), respectively, and b is the Langmuir adsorption constant ($L\ mg^{-1}$). K_F and $1/n$ are Freundlich constants related to the sorption intensity and adsorption capacity, respectively. According to the correlation coefficient in Table 4, R^2 values in Langmuir are the higher value (closed to unit) compared with Freundlich model for both adsorbents. So, the adsorption of Hg^{2+} metal ions on both of bioadsorbents fitted well to the Langmuir model. In this model, however, as aforementioned can be said that adsorption of Hg^{2+} ions was occurred on homogeneous surface of bioadsorbents as well as monolayer sorption. In other words, in this model only interaction between the adsorbate molecules and adsorbent is considered. The similar results had been reported by Senem Karahan et al. [30] and Dursun Saraydın et al. [31]. It can be also noted that the values of the "n" for both of the prepared adsorbents was bigger than unit and these values were between 1.523 and 2.823 at three studied temperatures (see Table 4). Furthermore, according to the Giles classification, S, L, and C type isotherms, these high values of "n" ($n > 1$ for both bioadsorbent) suggesting L type isotherm and indicating the physic-sorption process. It is noticeable that the presented "n" values by the Giles classification as following as: $n < 1$ correspond to S shape, $n = 1$ to C type, and $n > 1$ to L type [32].

In fact, in L-shape type with increasing concentration of solute (Hg^{2+} ions) and prolonging the contact time, adsorption capacity for both adsorbents increased sharply and that eventually slowed down gradually to reach equilibrium as it can be seen from Fig. 4c. It believed that with further passes of time, because saturation of the adsorption sites on the surface of the adsorbents remained vacant sites become more difficult to find with the progressive covering of the surface [33]. Therefore, based on the above results, it can be concluded that adsorption of Hg^{2+} ions by both biosorbents was as monolayer sorption and physically.

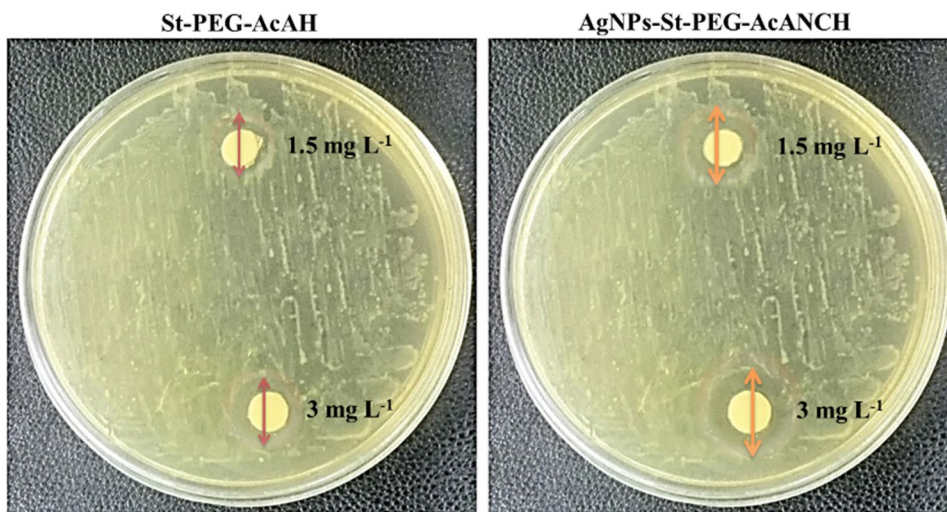
Table 4 Summary of isotherm parameters for the adsorption of mercury on St-PEG-AcAH and AgNPs-St-PEG-AcANCH

Isotherm model	Temperature (K)	Parameter	St-PEG-AcAH	AgNPs-St-PEG-AcANCH
Langmuir	288	q_m	188.679	263.157
		b	0.062	0.065
		R^2	0.997	0.983
	298	q_m	185.185	243.902
		b	0.121	0.162
		R^2	0.994	0.993
	308	q_m	181.818	232.558
		b	0.227	0.335
		R^2	0.999	0.985
Freundlich	288	KF	0.420	0.318
		n	2.823	2.207
		R^2	0.979	0.963
	298	KF	0.390	0.244
		n	2.669	1.831
		R^2	0.975	0.955
	308	KF	0.272	0.175
		n	2.082	1.523
		R^2	0.932	0.947

Evaluation of Antibacterial Activity

The antimicrobial effect (in vitro) of bioadsorbent was investigated by comparing the diameter of the growth inhibition zones of *E. coli*. As can be seen from Fig. 5, both AgNPs-St-PEG-AcANCH and St-PEG-AcAH showed the antibacterial effect on the bacteria, *E. coli*, after 24 h of incubation at 37 °C. So that, paper discs soaked for St-PEG-AcAH with two different concentration exhibited inhibition zone values of 3.83 mm (for 1.5 ppm) and 5.70 mm (for 3 ppm) against *E. coli*. Similarly, according to the figure, AgNPs-St-PEG-AcANCH exhibited inhibition zone values of 10.56 mm (for 1.5 ppm), and 13.32 mm (for 3 ppm) against *E. coli* with the same concentrations. In this study, the results obtained that the AgNPs-St-PEG-AcANCH showed further potential antibacterial activity than the St-PEG-AcAH under similar

Fig. 5 Antibacterial activities of St-PEG-AcAH and NPAg-AcANCH against *E. coli*



test conditions. This could be related to the smaller size of AgNPs and the presence of a more porous structure of nanocomposite hydrogel which during the swelling process released the silver nanoparticles efficiently into the media and led to its interaction with the lipid layer of the bacterial cell membrane [34]. Since gram-negative *E. coli* has a thin lipid layer of the cell wall may lead to a facilitate penetration of released silver nanoparticles into the bacterial cell membrane [35]. The released AgNPs can then destroy with the lipid layer of the cell membrane.

Conclusion

In short, St-PEG-AcAH and AgNPs-St-PEG-AcANCH was synthesized through free radical copolymerization in aqueous solution. Including Ag nanoparticles inside the St-PEG-AcAH was confirmed by multiple shifts in peak location of FTIR spectra of some functional groups such as carboxylic or carboxylate. The results of TGA showed the enhanced thermal stability of AgNPs-St-PEG-AcANCH in comparison with St-PEG-AcAH. XRD, AFM, and TEM techniques were also confirmed the presence of AgNPs and average particle size of 45 nm. The swelling changes and thereafter adsorption capacity of the optimized hydrogel and nanocomposite were examined in water, ethanol–water (30:70), ethanol–water (50:50), methanol–water (40:60), respectively. Reaching the maximum Hg^{2+} removals, determining the optimal bioadsorbent mass loaded 96.32% and 90.43% for AgNPs-St-PEG-AcANCH and St-PEG-AcAH, were performed in water solvent, respectively. The effect of pH on the adsorption of Hg^{2+} ions was investigated, and the maximum adsorption was observed at pH 7 for St-PEG-AcAH and 6 for AgNPs-St-PEG-AcANCH. The effect of initial concentration of Hg^{2+} ions were also evaluated in the range of 50–300 ppm at 298 K for St-PEG-AcAH and AgNPs-St-PEG-AcANCH,

and it was found that increasing the initial Hg^{2+} ions concentration from 50–300 ppm decreased the percentage removal ability of both bioadsorbents. The effect of temperature on Hg^{2+} ions removal was carried out at three different temperatures, i.e., 288 K, 298 K, and 308 K, which showed more effective sorption of Hg^{2+} ions on both of bioadsorbents at the highest temperature. Adsorption isotherms were utilized to explain the adsorption data by linear Langmuir and Freundlich isotherms. Based on the correlation coefficient, the adsorption trend of Hg^{2+} metal ions using both bioadsorbent followed by Langmuir model. On the other hand, based on the diffusion exponents ($n > 1$) and according to Giles classification system, L type sorption was found for both adsorbents. In addition, the results for antiracial activity of prepared hydrogels confirmed that AgNPs-St-PEG-AcANCH showed further potential antibacterial activity than St-PEG-AcAH under similar test conditions. This could be related to the smaller size of AgNPs and more porous structure of nanocomposite hydrogel led to its better interaction with the lipid layer of the bacterial cell membrane.

Acknowledgements The research leading to these results has received funding from the chemistry laboratory of Islamic Azad University, Tehran-North Branch.

References

1. Yu G, Lu Y, Guo J, Patel M, Bafana A, Wang X, Qiu B, Jeffries C, Wei S, Guo Z, Wujcik EK (2018) Carbon nanotubes, graphene, and their derivatives for heavy metal removal. *Adv Compos Hybrid Mater* 1:56–78
2. Irani M, Ismail H, Ahmad Z, Fan M (2015) Synthesis of linear low-density polyethylene-g-poly (acrylic acid)-co-starch/organo-montmorillonite hydrogel composite as an adsorbent for removal of Pb (II) from aqueous solutions. *J Environ Sci* 27:9–20
3. Sung JH, Back SK, Lee ES, Jang HN, Seo YC, Kang YS, Lee MH (2018) Application of powdered activated carbon coating to

- fabrics in a hybrid filter to enhance mercury removal. *J Environ Sci* 80:58–65
4. Likus-Ciešlik J, Pietrzykowski M, Chodak M (2018) Chemistry of sulfur-contaminated soil substrate from a former frash extraction method sulfur mine leachate with various forms of litter in a controlled experiment. *Water Air Soil Pollut* 229:71
 5. Song D, Yang R, Long F, Zhu A (2019) Applications of magnetic nanoparticles in surface-enhanced Raman scattering (SERS) detection of environmental pollutants. *J Environ Sci* 80:14–34
 6. Fersi Bennani C, M'hiri O (2015) Comparative study of the removal of heavy metals by two nanofiltration membranes. *Desalination Water Treat* 53:1024–1030
 7. Santhosh C, Velmurugan V, Jacob G, Jeong SK, Grace AN, Bhatnagar A (2016) Role of nanomaterials in water treatment applications: a review. *Chem Eng J* 306:1116–1137
 8. Li G, Zhao Z, Liu J, Jiang G (2011) Effective heavy metal removal from aqueous systems by thiol functionalized magnetic mesoporous silica. *J Hazard Mater* 192:277–283
 9. Meng Q, Chen H, Lin J, Lin Z, Sun J (2017) Zeolite a synthesized from alkaline assisted pre-activated halloysite for efficient heavy metal removal in polluted river water and industrial wastewater. *J Environ Sci* 56:254–262
 10. Tabesh S, Davar F, Loghman-Estarki MR (2018) Preparation of γ -Al₂O₃ nanoparticles using modified sol-gel method and its use for the adsorption of lead and cadmium ions. *J Alloy Compd* 730:441–449
 11. Lo IMC, Yin K, Tang SCN (2011) Combining material characterization with single and multi-oxyanion adsorption for mechanistic study of chromate removal by cationic hydrogel. *J Environ Sci* 23:1004–1010
 12. Ozay O, Ekici S, Baran Y, Aktas N, Sahiner N (2009) Removal of toxic metal ions with magnetic hydrogels. *Water Res* 43:4403–4411
 13. Wang X, Deng W, Xie Y, Wang C (2013) Selective removal of mercury ions using a chitosan–poly (vinyl alcohol) hydrogel adsorbent with three-dimensional network structure. *Chem Eng J* 228:232–242
 14. Lee S, Kim N, Cho S, Ryu JC, Cho Y, Park JA, Lee SH, Kim J, Choi JW (2017) Application of organic-inorganic hybrid composite particle for removal of heavy metal ions from aqueous solution and its toxicity evaluation. *Eur Polym J* 95:335–347
 15. Liu X, Gan H, Hu C, Sun W, Zhu X, Meng Z, Gu R, Wu Z, Dou G (2019) Silver sulfadiazine nanosuspension-loaded thermosensitive hydrogel as a topical antibacterial agent. *Int J Nanomed* 14:289–300
 16. Bhuyan MM, Okabe H, Hidaka Y, Hara K (2017) Pectin-[(3-acrylamidopropyl) trimethylammonium chloride-co-acrylic acid] hydrogel prepared by gamma radiation and selectively silver (Ag) metal adsorption. *J Appl Polym Sci* 135:1–14
 17. Firdaus F, Friezee-Idris MS, Yusof SF (2019) Adsorption of nickel ion in aqueous using rubber-based hydrogel. *J Polym Environ* 27:1770–1780
 18. Nematidil N, Sadeghi M (2018) Free radical synthesis of nanosilver/gelatin-poly (acrylic acid) nanocomposite hydrogels employed for antibacterial activity and removal of Cu (II) metal ions. *J Hazard Mater* 351:38–53
 19. Kiatkamjornwong S, Thakeow P, Sonsuk M (2001) Chemical modification of cassava starch for degradable polyethylene sheets. *Polym Degrad Stab* 73:363–375
 20. Alshehri SM, Aldalbahi A, Al-Hajji AB, Chaudhary AA, Panhais M, Alhokbany N, Ahamad T (2016) Development of carboxymethyl cellulose-based hydrogel and nanosilver composite as antimicrobial agents for UTI pathogens. *Carbohydr Polym* 138:229–236
 21. Siddiqui MN, Redhwi HH, IoannisTsagkalias L, Softas C, Ioannidou M, Achilias D (2016) Synthesis and characterization of poly (2-hydroxyethyl methacrylate)/silver hydrogel nanocomposites prepared via in situ radical polymerization. *Thermochim Acta* 643:53–64
 22. Mohamadi Zahedi S, Mansourpanah Y (2018) Construction of chitosan-carboxymethyl β -cyclodextrin silver nanocomposite hydrogel to improve antibacterial activity. *Plast Rubber Compos* 47:273–281
 23. Rao KM, Kumar A, Haider A, Han SS (2018) Biodegradable tragacanth gum based silver nanocomposite hydrogels and their antibacterial evaluation. *J Polym Environ* 26:778–788
 24. Saeedirad R, Ganjali ST, Bazmi M, Rashidi A (2018) Effective mesoporous silica-ZIF-8 nano-adsorbents for adsorptive desulfurization of gas stream. *J Taiwan Inst Chem Eng* 82:10–22
 25. Dawlet A, Talip D, Mi HY, Ti M (2013) Removal of mercury from aqueous solution using sheep bone charcoal. *Procedia Environ Sci* 18:800–808
 26. Crini G, Lichtfouse E, Wilson LD, Morin-Crini N (2018) Conventional and non-conventional adsorbents for wastewater treatment. *Environ Chem Lett* 17:195–213
 27. Jianqi F, Lixia G (2002) Swelling/deswelling behavior of thermally induced PVA/PAA hydrogel fiber in aqueous salt solutions. *J Polym Mater* 19(1):103–112
 28. Zohuriaan-Mehr MJ, Motazedi Z, Kabiri K, Ershad-Langroudi A, Allahdadi I (2006) Gum arabic-acrylic superabsorbing hydrogel hybrids: studies on swelling rate and environmental responsiveness. *J Appl Polym Sci* 102:5667–5674
 29. Li A, Wang A, Chen J (2004) Studies on poly(acrylic acid)/ata-pulgite superabsorbent composites. II. Swelling behaviours of superabsorbent composites in saline solutions and hydrophilic solvent-water mixtures. *J Appl Polym Sci* 94:1869
 30. Karahan S, Yurdakoç M, Seki Y, Yurdakoç K (2006) Removal of boron from aqueous solution by clays and modified clays. *J Colloid Interface Sci* 293:36–42
 31. Saraydın D, Işıkver Y, Karadağ E (2018) A Study on the correlation between adsorption and swelling for poly (Hydroxamic Acid) hydrogels-triarylmethane dyes systems. *J Polym Environ* 26:3924–3936
 32. Giles CH, Mawan TH, Nakhwa SN, Smith D (1960) Studies in sorption. Part XJ. A system of classification of solution adsorption isotherms. *J Chem Soc.* <https://doi.org/10.1039/JR9600003973>
 33. Charles H, Smith G, Smith D (1974) A general treatment and classification of the solute adsorption isotherm I. theoretical. *J Colloid Interface Sci* 47:755–765
 34. Basu S, Samanta HS, Ganguly J (2018) Green synthesis and swelling behavior of Ag-nanocomposite semi-IPN hydrogels and their drug delivery using dolichos biflorus Linn. *Soft Mater* 16:7–19
 35. Lakshminarayanan R, Ye E, Young DJ, Li Z, Loh XJ (2018) Recent advances in the development of antimicrobial nanoparticles for combating resistant pathogens. *Adv Health Mater* 7(13):1701400

Publisher's Note Springer Nature remains neutral with regard to jurisdictional claims in published maps and institutional affiliations.